



RESEARCH ARTICLE

Ultra-robust stretchable electrode for e-skin: In situ assembly using a nanofiber scaffold and liquid metal to mimic water-to-net interaction

Jinwei Cao^{1,2,3,4} | Fei Liang^{5,6} | Huayang Li^{1,2,3} | Xin Li⁵ | Youjun Fan^{5,7} |
 Chao Hu^{2,3} | Jing Yu⁴ | Jin Xu¹ | Yiming Yin¹ | Fali Li^{2,3} | Dan Xu^{2,3} |
 Hanfang Feng¹ | Huali Yang^{2,3} | Yiwei Liu^{2,3} | Xiaodong Chen⁴ |
 Guang Zhu^{1,5}  | Run-Wei Li^{2,3} 

¹New Materials Institute, Department of Mechanical, Materials and Manufacturing Engineering, University of Nottingham Ningbo China, Ningbo, China

²CAS Key Laboratory of Magnetic Materials and Devices, Ningbo Institute of Materials Technology and Engineering, Chinese Academy of Sciences, Ningbo, China

³Zhejiang Province Key Laboratory of Magnetic Materials and Application Technology, Ningbo Institute of Materials Technology and Engineering, Chinese Academy of Sciences, Ningbo, China

⁴Innovative Center for Flexible Devices (iFLEX), Max Planck-NTU Joint Lab for Artificial Senses, School of Materials Science and Engineering, Nanyang Technological University, Singapore, Singapore

⁵CAS Center for Excellence in Nanoscience, Beijing Key Laboratory of Micro-Nano Energy and Sensor, Beijing Institute of Nanoenergy and Nanosystems, Chinese Academy of Sciences, Beijing, China

⁶Institute of Textiles & Clothing, The Hong Kong Polytechnic University, Hong Kong, China

⁷State Key Lab of New Ceramics and Fine Processing, School of Materials Science and Engineering, Tsinghua University, Beijing, China

Correspondence

Guang Zhu, New Materials Institute, Department of Mechanical, Materials and Manufacturing Engineering, University of Nottingham Ningbo China, Ningbo 315100, China.

Email: guang.zhu@nottingham.edu.cn

Run-Wei Li, CAS Key Laboratory of Magnetic Materials and Devices, Ningbo Institute of Materials Technology and Engineering, Chinese Academy of Sciences, Ningbo 315201, China.

Email: runweili@nimte.ac.cn

Funding information

National Key R&D Project from Ministry of Science and Technology, Grant/Award Number: 2016YFA0202703; National Natural Science Foundation of China, Grant/Award Numbers: 51525103,

Abstract

The development of stretchable electronics could enhance novel interface structures to solve the stretchability–conductivity dilemma, which remains a major challenge. Herein, we report a nano-liquid metal (LM)-based highly robust stretchable electrode (NHSE) with a self-adaptable interface that mimics water-to-net interaction. Based on the in situ assembly of electrospun elastic nanofiber scaffolds and electrosprayed LM nanoparticles, the NHSE exhibits an extremely low sheet resistance of 52 mΩ sq⁻¹. It is not only insensitive to a large degree of mechanical stretching (i.e., 350% electrical resistance change upon 570% elongation) but also immune to cyclic deformation (i.e., 5% electrical resistance increases after 330 000 stretching cycles with 100% elongation). These key properties are far superior to those of the state-of-the-art reports. Its robustness and stability are verified under diverse circumstances, including long-term exposure to air (420 days), cyclic submersion (30 000 times), and resilience against mechanical damages. The

Jinwei Cao, Fei Liang, and Huayang Li contributed equally to this work.

This is an open access article under the terms of the Creative Commons Attribution License, which permits use, distribution and reproduction in any medium, provided the original work is properly cited.

© 2022 The Authors. *InfoMat* published by UESTC and John Wiley & Sons Australia, Ltd.

51701231, 51931011; Ningbo Municipal 3315 Talent Scheme and Ningbo Scientific and Technology Bureau; Zhejiang Provincial Natural Science Foundation of China, Grant/Award Number: LR19F010001; K.C. Wong Education Foundation, Grant/Award Number: GJTD-2020-11

combination of conductivity, stretchability, and durability makes the NHSE a promising conductor/electrode solution for flexible/stretchable electronics for applications such as wearable on-body physiological signal detection, human-machine interaction, and heating e-skin.

KEYWORDS

crack confinement, functional e-skin, in situ assembly, self-adaptable interface, ultra-robust stretchable electrode

1 | INTRODUCTION

Robust and stable soft conductors are highly desirable for precise electric signal transmission as well as long-term dynamic services in smart wearable electronics, such as epidermal electronics,^{1–4} implantable sensors,^{5,6} optoelectronics devices,^{7,8} neuroprosthetics,⁹ energy-storage devices,¹⁰ and soft robotics.¹¹ Furthermore, in epidermal electronic systems, stretchable electrodes are of paramount significance for the stable collection of human electrophysiological signals, for example, electrocardiography (ECG),¹² electromyography,¹³ and electroencephalogram.¹⁴ Notably, to achieve precise and stable physiological signal sensing in complex environments, it is essential for epidermal electrodes to possess excellent and robust electrical conductivity under various dynamic conditions, including mechanical deformation, temperature variation, perspiration soaking, and submersing.

Until now, stretchable electrodes have been categorized into three major types,^{15,16} namely, structure-based stretchable electrodes,¹⁷ intrinsically stretchable conductors,¹⁸ and composite-based stretchable electrodes.¹⁹ Jang et al. prepared a three-dimensional (3D) helical microcoil layout to offer elastic mechanics for advanced components interconnection.²⁰ Wang et al. pioneered the development of a poly(3,4-ethylenedioxythiophene):poly(styrenesulfonate) (PEDOT:PSS) film to realize a high conductivity of 4100 S cm⁻¹ under 100% stain.²¹ Jin et al. developed ink-permeated stretchable e-textiles that presented 7000% resistance variation under 450% elongation.²² However, these stretchable electrodes are still not robust enough under high strain or cyclic stretching.

Recently, liquid metal (LM), generally nontoxic gallium-based alloys,²³ has emerged as a possible solution, for example, a 3D-Calabash bunch conductive network.²⁴ Although the high surface tension of LM and poor interface interaction between LM and elastomers make it challenging to maintain conductivity under large strain,²⁵ two major methods have been developed to enhance the adhesion between LM and elastomers, that is, alloying LM with other elements (AgNP-Ga-In or AuGa₂)^{26,27} and adding binder materials to form hydrogen bonds (fructose or hydrogel).^{28,29} However, these methods failed to achieve a breakthrough in robust stretchable electrodes when serving in

long-term healthcare systems.^{30,31} Thus, it is still a major challenge to simultaneously achieve electrical stability upon stretching and cyclic durability for LM-based stretchable electrodes.

Herein, we demonstrate a nano-LM-based high-robust stretchable electrode (NHSE) via in situ assembly of electrospun fibrous elastic scaffolds (thermoplastic polyether urethanes, TPU) and electrospayed LM nanoparticles. An ultra-low sheet resistance of 52 mΩ sq⁻¹ was achieved with a standard deviation of 5 mΩ sq⁻¹. The NHSE exhibited excellent electromechanical properties with only 350% resistance variation under an elongation of 570%. This outstanding property is attributed to a self-adaptable interface between the LM and the nanofiber scaffolds, which mimics the water-to-net interaction. Under a small strain (<100% elongation), the interface stress is relaxed owing to the flow of the LM, inhibiting the formation of cracks and maintaining a continuous LM film. Under a large strain (100%–500%), the nanofiber scaffold serves as a local confining boundary that impedes crack propagation. More importantly, the NHSE delivers superior robustness against dynamic cyclic stretching and environmental stimuli (i.e., heating, acid and alkali exposure, and submersing). Specifically, it demonstrates only a 5% resistance variation after 330 000 stretching cycles at a 100% cyclic strain, which shows superior robustness to other recently reported electrodes. Using the ultrathin and highly robust NHSE, we successfully fabricated wearable devices for long-term ECG monitoring, electrothermal heater, strain-insensitive, and wearable human-machine interface system for computer game instruction input. These contribute to the future development of Internet of Things (IoT)-based wearable healthcare monitoring systems and skin-like human-machine interfaces.

2 | RESULTS AND DISCUSSION

2.1 | Preparation of the NHSE and its static electrical performance

The fabrication process of the NHSE is shown in Figure 1A. The TPU nanofibers were electrospun from a

TPU-hexafluoroisopropanol (HFIP) solution, which generated fine (~600 nm in diameter, Figure S1) and robust nanofibers.³² The LM nanoparticles were dispersed in an ice-bathed isopropanol solution that enabled stable LM

nanoparticle suspension³³ to facilitate subsequent mechanical activation process (Figure S2). Then, the TPU nanofibers and the LM nanoparticles were collected on a metal collector simultaneously by electrospinning and

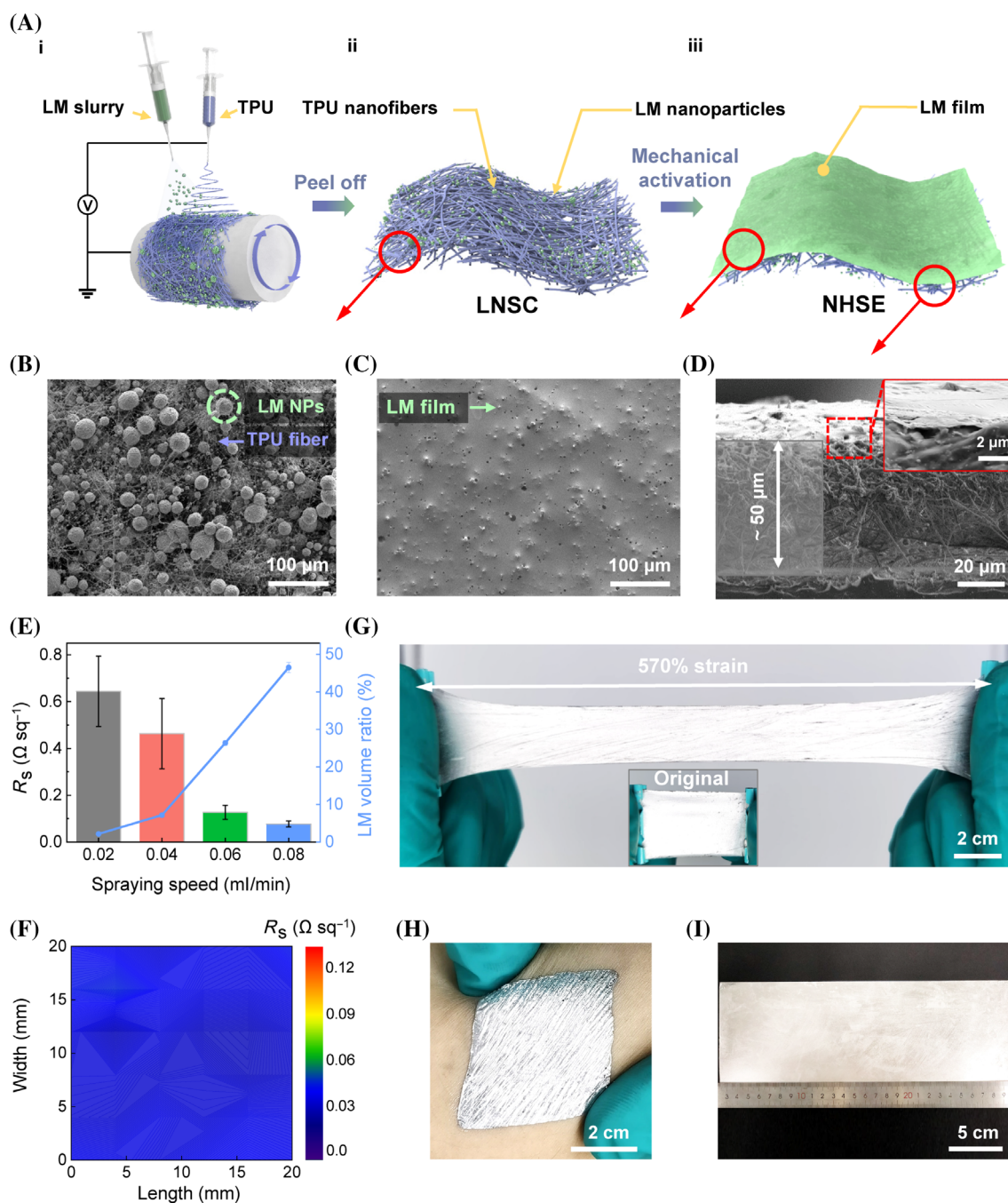


FIGURE 1 Design of nano-LM-based high-robust stretchable electrode (NHSE) and its static electrical performance. (A) Schematic illustration of the (i) electrospinning and electrospinning process to fabricate (ii) the LM nanoparticles @ TPU scaffold composite (LNSC) that is subsequently activated to form (iii) the NHSE. (B, C) Top-down view SEM of the LNSC and the NHSE, respectively. (D) Cross-sectional SEM images of the LM membrane. (E) Sheet resistance of the NHSE and volume ratio of LM in the LNSC as a function of EGaIn nanoparticles solution electrospinning speed. (F) Area mapping of sheet resistance distribution of the NHSE with a size of 20 × 20 mm². (G) Photographs of NHSE under relaxed (inset) and 570% of elongation. (H) Picture of the highly conformal NHSE attached on the forearm. (I) A size of 10 cm × 30 cm NHSE shows its promising utility for the electrode large-scale production

electrospraying, respectively (Figure 1A,i). After this process, the LM nanoparticles were bonded onto the TPU nanofibers to form an LM nanoparticle/TPU scaffold composite (LNSC) (Figure 1A,ii). As revealed by the top-down view of the scanning electron microscopy (SEM) (Figure 1B), the LM nanoparticles were composed of nano-sized and micro-sized particles that might be agglomerated from smaller ones. These LM nanoparticles densely adhered to the TPU nanofiber scaffold due to size effect (detailed in Figure S3). To break the oxide shell of the LM nanoparticles and achieve a conductive pathway, an external stimulus, for example scraping, was conducted on top of the specimen for the coalescence of the LM nanoparticles. Consequently, an ultrathin, highly conductive LM film on the top part was formed, as shown in Figure 1A,iii. The LM film showed a continuous morphology (Figure 1C), which was supported by the porous nanofiber-based scaffold underneath. This phenomenon is due to the balance between the Laplace capillary force (F_l) and the gravitational force (F_g), as illustrated in Figure S4. It has the same nature as the water-to-net interaction in the macroscopic world. The overall thickness of the NHSE is $\sim 50 \mu\text{m}$, including an ultrathin LM membrane with a thickness of hundreds of nanometers on the top (Figure 1D). The LM nanoparticle fabrication may lessen the surface tension of the LM, enabling its membrane to be thinner than those in other works.^{29,34}

The NHSE exhibits excellent intrinsic electrical performance, as illustrated in Figure 1E,F. Specifically, the LNSC possesses a low volume ratio of LM, which were only 2.18%, 7.18%, 26.42%, and 46.51% for the electrospraying rates of 0.02, 0.04, 0.06, and 0.08 ml min^{-1} , respectively. Notably, the mass loading of LM in various spray speeds is also measured to illustrate its absolute content, that is, 0.60 (± 0.17), 2.24 (± 0.002), 7.96 (± 0.69), and 14.01 (± 1.34) mg cm^{-2} for these four parameters (Figure S5A–D). The sheet resistance decreased owing to the larger quantity of LM and reached as low as 52 $\text{m}\Omega \text{sq}^{-1}$ at $\sim 46.5\%$ volume ratio of LM particles, as presented in Figure 1E. Based on the mapping of the sheet resistance in an area of $2 \times 2 \text{ cm}^2$, a standard deviation of 5 $\text{m}\Omega \text{sq}^{-1}$ was obtained (Figure 1F). As the TPU scaffold enables exceptional mechanical stretchability and mechanical compliance, the NHSE shows stretchability with a uniaxial elongation of $\sim 570\%$ (Figures 1G and S6). As illustrated in Figure 1H, it forms a seamless and conformal contact with the human forearm without adhesives. No exfoliation was observed upon dynamic deformation of the skin. In addition, the fabrication process is compatible with possible area-scalable production, as demonstrated by a sample with dimensions of $10 \text{ cm} \times 30 \text{ cm}$ (Figure 1I).

2.2 | Electrical characterization of the NHSE under mechanical and environmental stimuli

The stability and robustness under mechanical deformation are the most critical criteria for stretchable electrodes, which have been highlighted in recent studies.^{35,36} The superior performance of the NHSE lies in three aspects. First, its electrical resistance is insensitive to large mechanical stretching. Second, the electrical resistance remains stable despite several cyclic deformations. Third, it shows a high level of robustness against diverse environmental conditions, for example fluid soaking with different pH values, repeated submersing, temperature variation, and long-time air exposure. The detailed results are presented below.

First, the electrical resistance was monitored by uniaxial stretching. For the sample with a mass loading of 14.01 (± 1.34) mg cm^{-2} , the resistance increased by only 52% and 350% at elongations of 100% and 570%, respectively (Figure 2A). In comparison, the resistance variation was found to be in the range of 1000%–8000% at an elongation range of 300–600% in very recent state-of-the-art works.^{1,22,36,37} In addition, the resistance can almost immediately recover to its original value once the stretching is released. For example, if a sample undergoes five stretching cycles as follows: 0% \rightarrow 100% \rightarrow 0% \rightarrow 200% \rightarrow 0% \rightarrow 300% \rightarrow 0% \rightarrow 400% \rightarrow 0% \rightarrow 500% \rightarrow 0% (Figure 2B), there are only 18% (47 $\text{m}\Omega$) and 290% (730 $\text{m}\Omega$) resistance variations after the first and fifth cycles, respectively. Figure 2C shows the sheet resistance versus the mechanical stretchability. With a combination of stretchability and conductivity, the NHSE in this work is superior to the most recently reported composite-based stretchable electrodes,^{22,24,38–44} including LM-elastomer composite (e.g., Fe-LM and Ag-LM) and Au-LM composites (e.g., Ag flakes, Ag NWs, and conductive polymers).

Second, the NHSE possesses exceptional electrical stability under dynamic cyclic deformation, as illustrated in Figure 2D–F. Instead of a resistance increase in the first stretching, the baseline resistance increased by only 5% in the subsequent 330 000 cycles to 100% elongation at 2 Hz (Figure 2D). This slight increase is possibly owing to the formation of the microscale wrinkles on the NHSE from plastic deformation upon $\sim 35\%$ strain (Figures S6 and S7A–C), which induces a prolonged conductive pathway. Interestingly, the resistance variation becomes smaller as more stretching cycles are applied (Figure 2D insets). This can also be explained by micro-wrinkles, which have been known for mitigating effective strain applied on stretchable devices.^{45,46} In addition, the resistance varied by $\sim 12\%$ after the cycles, making the NHSE

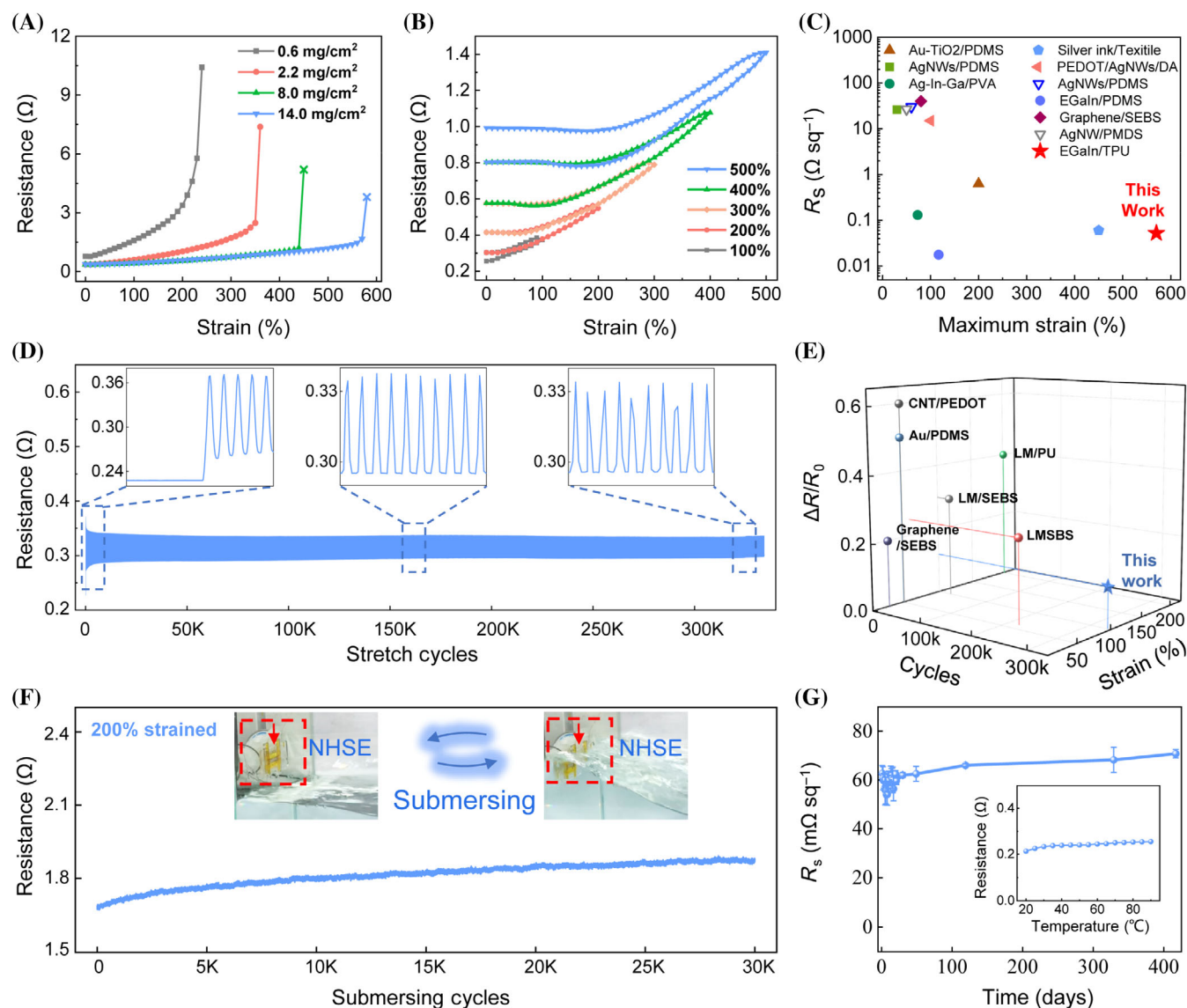


FIGURE 2 Electrical characterization of the NHSE under mechanical and environmental stimuli. (A) Resistance-strain character of the NHSE with various mass loadings of the LM particle (sample size: $1 \text{ cm} \times 1 \text{ cm}$). (B) Resistance variation of the NHSE against stretching cycles as $0\% \rightarrow 100\% \rightarrow 0\% \rightarrow 200\% \rightarrow 0\% \rightarrow 300\% \rightarrow 0\% \rightarrow 400\% \rightarrow 0\% \rightarrow 500\% \rightarrow 0\%$ (sample size: $1 \text{ cm} \times 1 \text{ cm}$, strain speed: $45\%/ \text{min}$). (C) Comparison of the initial sheet resistance and stretchability with previously published electrodes. (D) Resistance of the NHSE that lasted for $\sim 330\,000$ stretching cycles under 100% strain (0.2 Hz , sample size: $1 \text{ cm} \times 1 \text{ cm}$). The insets show the detailed resistance values at the beginning, in the middle, and at the end of the cyclic tensile test. (E) Comparison of resistance variation for recently published stretchable electrode under cyclic deformation. (F) The resistance of the 300% -stretched NHSE during $30\,000$ water submersing cycles (initial sample size: $1 \text{ cm} \times 1 \text{ cm}$). (G) Sheet resistance of the NHSE as exposed in the air for 420 days, and the inset shows the resistance variation of the NHSE under an increasing temperature from 20 to 90°C

among the most robust electrodes in recent state-of-the-art works^{34,36,43,44,47–50} (Figure 2E, Movie S1, Tables S1 and S2). Moreover, the normalized electrical resistance changes merely against twisting, bending, and $25\,000$ -bending cycles, as shown in Figure S8.

Third, the NHSE maintained almost constant resistance when stretched at 0% , 100% , or 200% under different environmental conditions (Figures 2F, S9, and S10).

The resistance of the stretched NHSE barely changed after 1000 -submersion cycles (Figure S9). A resistance increase of only 11% was observed for a 200% -stretched NHSE after $30\,000$ -submersing cycles (Figure 2F). In addition, samples soaked in artificial perspirations at pH 4.7 and 8.8 presented a negligible resistance increase (Figure S10A,B). As for the long-term stability of the NHSE in ambient environment, the sheet resistance

remained approximately $60 \text{ m}\Omega \text{ sq}^{-1}$ with a negligible variation upon exposure to air after 420 days (Figure 2G). Further, the resistance stability of the NHSE was investigated through heating processes (Figure 2G inset). The resistance of the NHSE gradually increased by 50% as the sample temperature was varied from 20 to 90°C . This increase is possibly due to the oxidation of the LM surface at elevated temperatures.

2.3 | Mechanism of the electrical robustness of the NHSE

Nature always enlightens us through various wonderful workmanships in material design and mechanism analysis.⁵¹ The NHSE highly resembles a natural phenomenon, in which a continuous water membrane spreads across a meshed fishing net (Figure 3A). As a strain is

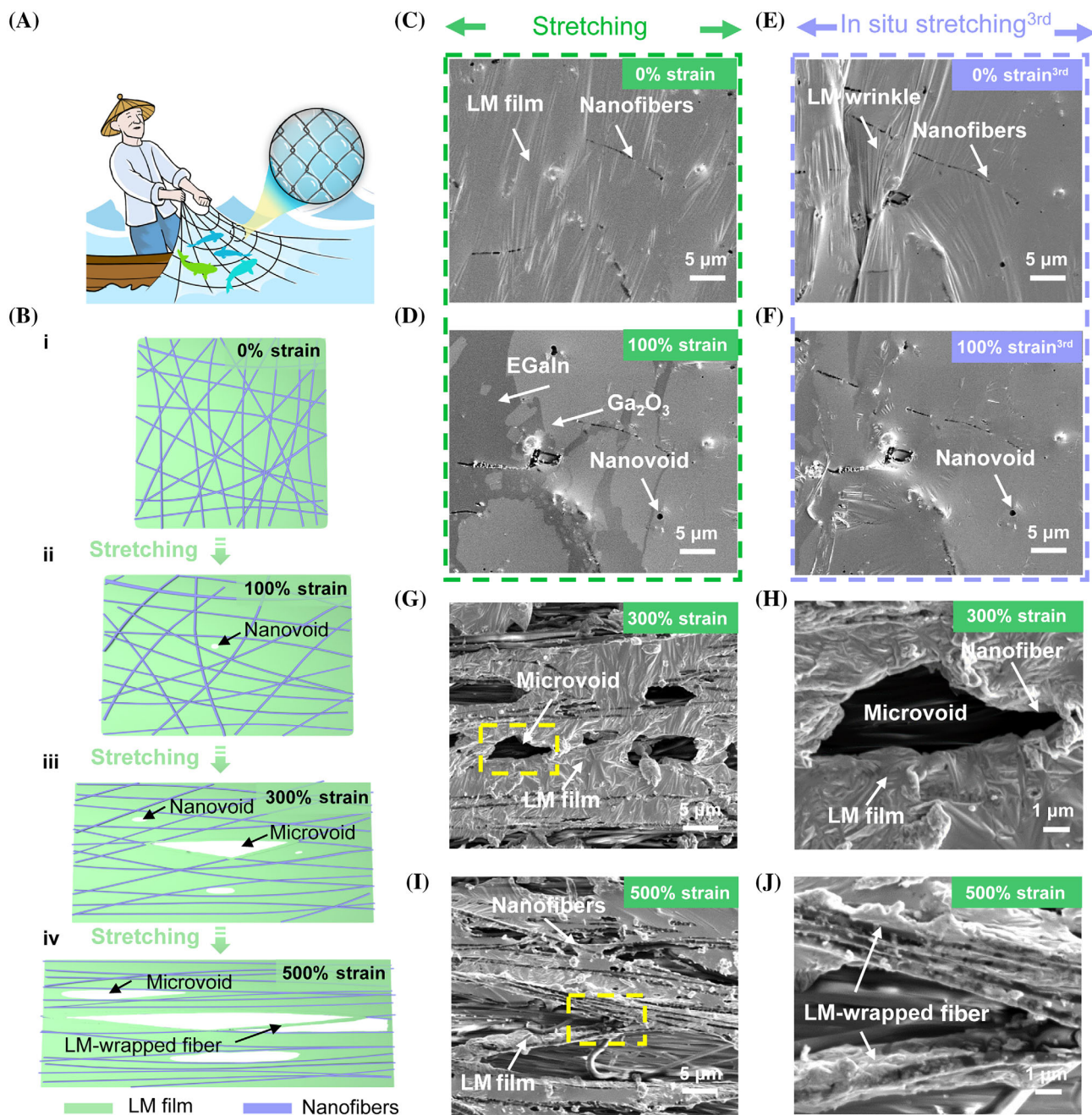


FIGURE 3 Self-adaptable interface between the LM membrane and TPU scaffold. (A) The zoom-in morphology of water membrane when a fisherman pulls a fishnet from the sea. (B) The self-adaptable interface evolution as stretched to 100%, 300%, and 500% strain, respectively. (C–F) In situ micromorphology analysis of the NHSE under 1st 100% strain stretching (C, D) and 3rd 100% strain stretching (E, F). (G, H) Micromorphology of the NHSE under 300% elongation. (I, J) Micromorphology of the NHSE under 500% elongation. [Correction added on 14 March 2022, after first online publication: Figure 3 has been updated.]

applied, the evolution of the interaction between the water membrane and the meshed net is illustrated in Figure S11A–C. The water membrane is deformable and maintains continuity during the initial stage of the strain. Under a large strain, if cracks are generated, they are confined within individual mesh units without causing fatal rupture of the water membrane.

Similar observations were found for the NHSE. To reveal the morphology evolution, samples with different levels of strains were examined by the SEM (Figure 3B–J). Here, the interface between the LM and the nanofibers is adaptable upon deformation, which is the key to the high level of electrical stability of the NHSE. This adaptable behavior is presented in two stages, as shown in Figure 3B. The first stage involves a small strain range when the elongation is less than 100%. In this stage, the morphology of the LM membrane evolves along with the deformation of the nanofibers without the build-up of the interface stress. As a result, the LM membrane remains integral, which is justified by the SEM image as well as a video with in situ stretching of 100% elongation (Figure 3C,D and Movie S2). Although random nanovoids could be identified (Figure 3D), neither proliferation nor propagation of the nanovoids was observed in subsequent stretching cycles (Figure 3E,F). In the second stage, in which the elongation increases beyond 100%, more nanovoids were generated, and they simultaneously expanded to micro-scale voids. However, the microvoids did not propagate throughout the entire LM membrane. Instead, they are confined locally by the nanofibers, which act as a boundary for isolating the microvoids from the surrounding area (Figure 3G,H). This confinement effect prevents the LM membrane from rupturing and preserves the active conducting pathways. Even if the elongation reaches 500%, the confinement is still effective despite the largely expanded and distorted voids, which is consistent with the results in Figure 2B. As a result, the NHSE remains functional. The distortion observed in Figure 3I,J is due to the re-orientation of the nanofibers under a uniaxial strain. The alignment of the nanofibers was quantitatively characterized by the SEM images and the 2D fast Fourier transform plots in Figures S12 and S13.⁵²

Based on the above analysis, the self-adaptable interfacial interaction is the key that enables the insensitivity and robustness of the electrical resistance against strain. To obtain this particular interface, the in situ assembly fabrication method in this work plays a vital and irreplaceable role. By dispersing the LM nanoparticles inside the TPU scaffold, the resulting material efficiently presents a spreading feature of LM to easily form a continuous film, which has also been verified in other work described as “ink-jettable carrier solvent”.⁵³ To prove this

point further, control experiments with other typical fabrication methods were conducted. In the first group, LM droplets were dropped onto a commercial TPU substrate and scratched across the substrate to form a continuous film (Movie S3). Without the self-adaptable interface, the LM film is broken into separated islands under an elongation of 100%, which is an irreversible failure (Figure S14). In the second group, a TPU-nanofiber-based scaffold was used as a substrate, and the LM droplets were subsequently applied via the same procedure as in the first group. This fabrication method has also been reported in a very recent work.³⁴ The reported results showed that the electrical resistance of the stretchable electrode changed by 30% after 25 000 stretching cycles (100% elongation). In contrast, the NHSE in this study experienced only a 12% variation in the electrical resistance after 330 000 stretching cycles.

2.4 | Application of the NHSE for stretchable conductor and ECG recordings

The NHSE depicted excellent potential for use as an interconnect in elastic electronic systems. For demonstration, it was applied as an elastic conductor to power a stripe of light-emitting diodes (LEDs) (~75 LEDs), as presented in Figure S15A,B in the Supporting Information. It was stretched from the original dimensions to an elongation of approximately 500%. A negligible variation in the LED brightness was observed. Repeatability was demonstrated through multiple stretching cycles. However, the brightness of the LED remained constant (Movie S4).

Biocompatibility is crucial for the NHSE when it serves as an e-skin in the human epidermal system. The low cytotoxicity of the NHSE was verified via an in vitro study by comparing the proliferation and morphology of human dermal fibroblast cells. The fluorescent live/dead staining images showed a similar density and equivalent morphology in the control and test media (Figure 4A). Nearly no dead cells were observed in our test group with a cell viability of ~95% after 24 h (Figure 4B).

Owing to its ultrathin and mechanically compliant nature, the NHSE is also suitable for use in epidermal devices for on-body physiological signal collection (Figure 4C–I and Movie S5). In the following demonstration, the NHSE forms a tight and conformal bonding on the human skin via the van der Waals force⁵⁴ and is used as an epidermal electrode for ECG recording. It has a contact impedance comparable to that of a commercial AgCl gel electrode (Figure 4C). In a static state, the signal obtained from the NHSE is equivalent to that of the commercial gel electrode (Figure 4D,E). Notably, more

flattened T peaks are achieved by the NHSE owing to its higher impedance in the range of 10–1000 Hz compared to the commercial electrodes. However, based on the ECG electrode sensitivity definition,⁵⁵ the sensitivity of the NHSE (0.43) is higher than that of the commercial electrodes (0.36). Specifically, the key advantage of the

NHSE for this application lies in stable signal detection under external disturbance. Figure 4F,G shows that the signal recording was accompanied by wrist movements. As a result, baseline fluctuation was observed for the gel electrode, while the signal from the NHSE remained unchanged. If water was poured onto the gel electrode

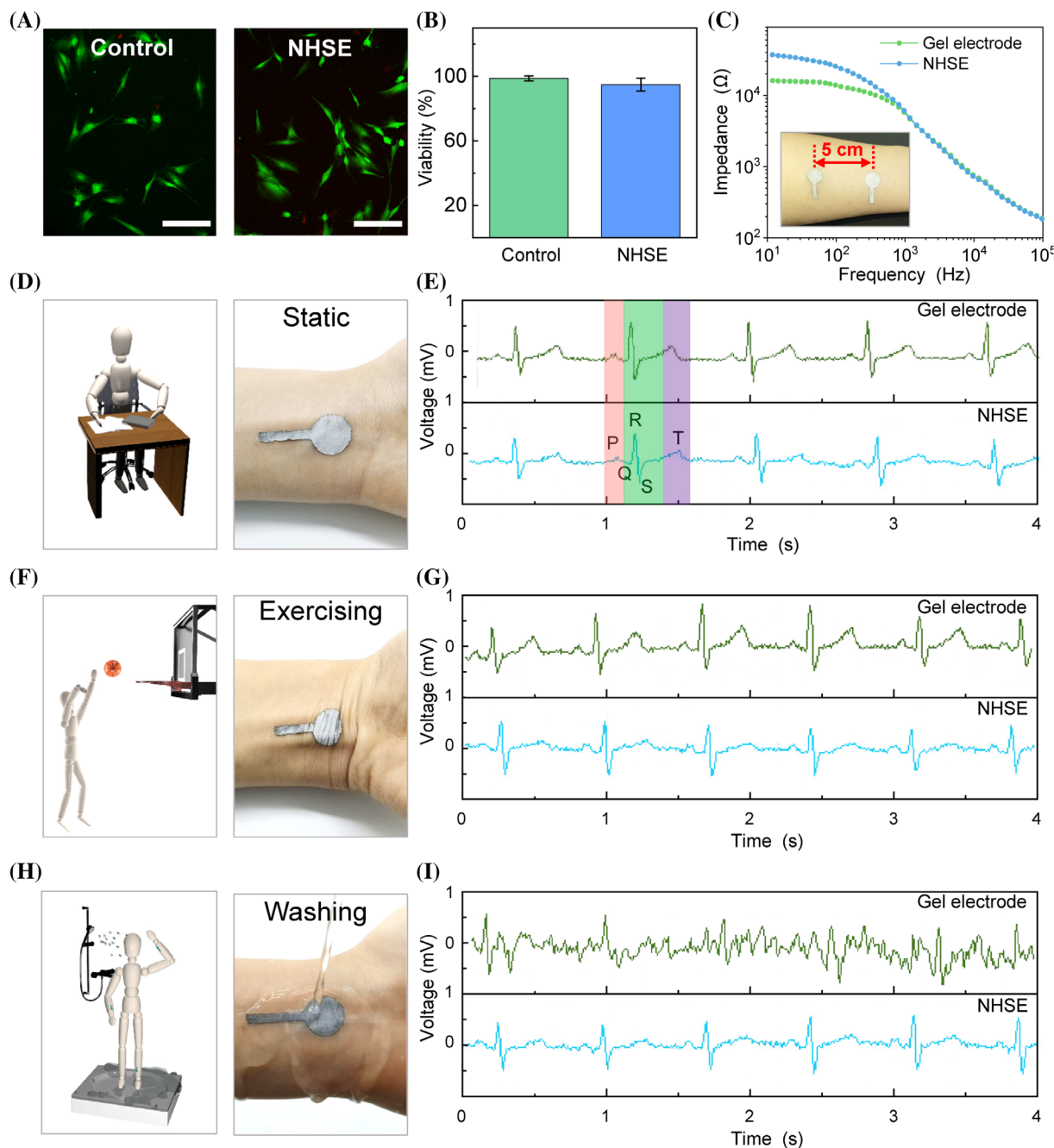


FIGURE 4 Application of the NHSE in ECG monitoring. (A) Fluorescent images of stained human dermal fibroblast cells that were cultured in media with control sample and NHSE sample. (B) Comparison of cell viability in different incubation groups. All the data in (B) are presented as mean \pm standard deviation. (C) Comparison of electrode-skin contact impedance of the NHSE and commercial gel electrode. (D–I) Schematics photographs of the NHSE for on-body healthcare monitoring and corresponding signals of commercial gel electrode (upper) and the NHSE (lower) while servicing in three scenes, that is, working statically (D, E), doing exercise (F, G), and taking a shower (H, I), respectively

during signal recording, significant noise buried the signal without recognizable regular patterns (Figure 4H,I). In contrast, the key features from the NHSE, that is P-waves, QRS complex, and T-waves, were still preserved and remained diagnosable. This contrast is attributed to the seamless and conformal on-body contact from the NHSE.

2.5 | Application of the NHSE for human-machine interface and electrothermal heater

The structure of the LM nanoparticles embedded in the TPU scaffold composite ensures two accesses in post-processing, that is partial activation and laser cutting. As a result, a monolithic multifunctional e-skin with two layers was successfully fabricated using these two methods. As presented in Figures 5A and S16A,B, this two-layer e-skin includes a deformation adaptive human-machine interactive system (top layer) and an electrothermal heater (bottom layer) with stretchability, conformality, and robustness, realizing a human-machine interface and continuous thermotherapy. The top layer, a capacitive sensor array, could input commands of up, down, left, right, and blank when connected to a wireless control module (Figure 5B). The haptic response mechanism is shown in Figure S17. Figure 5C shows a schematic diagram of this integrated system, which consists of six procedures: action instruction, AC-based capacitive signal variation, analog-digital signal conversion, signal processing by a microcontroller unit, and signal transmission to a PC by a Bluetooth module. This e-skin human-machine interactive system deforms conformably as patched on hand and remains functional even upon stretching owing to its conformality and robustness (Figure 5D,E and Movie S6). In addition, this device realizes the input of numbers on the wrist without any unexpected signals under positive or negative bending.

On the bottom layer, a serpentine heater exhibits extreme electrothermal robustness in wearable heating applications. The sample showed a rapid response to temperature upon power-driven. The corresponding temperatures were adjustable (from 35 to 93°C) by applying different voltages of 1, 2, 2.5, 3, 3.5, and 4 V (Figure 5G). The temperature of the heater remains stable after approximately 15 s and only changes by 8% (from 35.9 to 32.9°C) as the sample was stretched to 100% strain (Figure 5H and Movie S7). The temperature of the heater returned to its original level after being released. In the heating cycle experiments, our NHSE-based serpentine heater demonstrated durable heating performance (Figure 5I).

2.6 | Instant reconstruction of conductive pathway in the NHSE

The robustness of the NHSE is further verified as it survives from severe damages, including cutting and hole punching. As demonstrated in Figure 5J, a piece of NHSE was selectively and locally activated by drawing a line on top of the sample. This line became conductive following Ohm's law and was used as a flexible circuit to power the LED (Figure S18). The conductive line was cut using a razor blade on the left side of the LED. Subsequently, hole punching was conducted on the other side of the LED. During and after the above operation, the LED was still lighting (Figure 5J). The damaged flexible circuit remained functional even after stretching (Figure 5K).

This observation is due to the reconstruction of the conductive pathways at the damaged sites. As illustrated in Figure S19A, the line in the middle of the sample represents the region where the activation has taken place. The rest of the area is subjected to subsequent activation upon mechanical stimuli. Although cutting or punching disconnects the original conductive pathway, it essentially activates new sites around the cutting/punching mark (Figure S19B,C). As a result, a fresh conductive pathway is reconstructed simultaneously when damage occurs, which enables an uninterrupted power supply. As quantitatively revealed in Figure S20A, a fivefold increase in the electrical resistance is observed after the first cut, as well as another 400% and 600% increases after the second and third cuts, respectively. Similar observations occurred in the case of the successive hole punching (Figure S20B). Therefore, the NHSE exhibits an exceptional level of robustness despite severe damages.

3 | CONCLUSION

We proposed a nano-LM-based highly robust stretchable electrode based on liquid metal nanoparticles and a TPU nanofiber scaffold by mimicking the water-to-net interface for long-term dynamic human healthcare monitoring and electrically self-healing stretchable connectors. Without alloying or adding binder materials, the as-prepared NHSE realizes a self-adaptable interface, through which the LM membrane remains continuous under a strain range below 100%, and the LM voids are confined locally by the nanofibers under a larger strain of up to 500%. Thus, this self-adaptable interfacial interaction realizes an unprecedented combination of super-low resistance under high elongation and exceptional electrical robustness upon cyclic external stimuli. These are essential characters that contribute to the all-day on-body ECG monitoring under three scenarios: staying static,

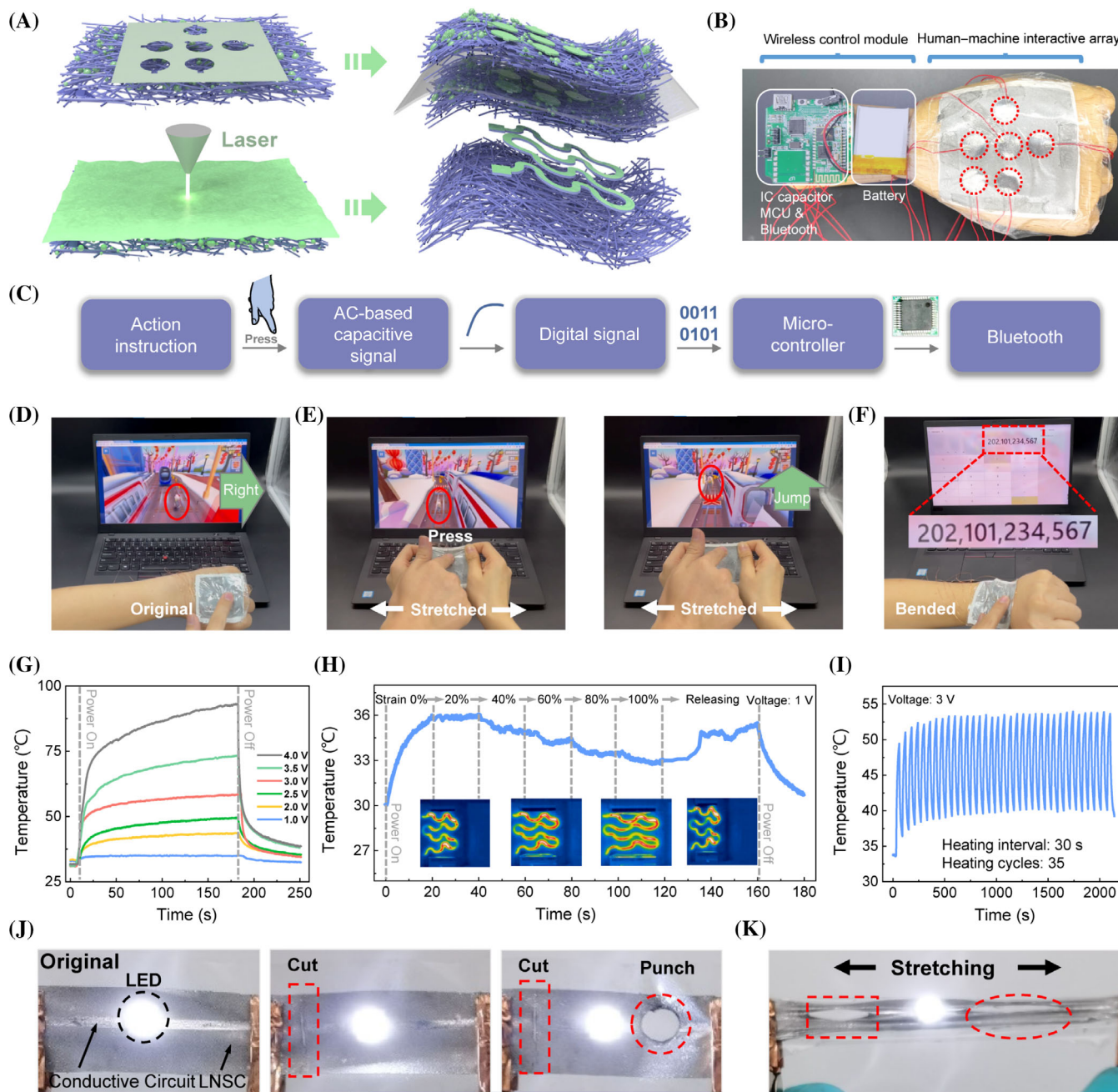


FIGURE 5 Application of the NHSE in the e-skin human-machine interactive system, stretchable serpentine heater, and robust circuits against mechanical damages. (A) Schematic illustration of two post-processing methods for the NHSE, that is partial activation and laser cutting. (B) Photographs of the e-skin human-machine interactive array and wireless control module. The insets red marks present the functional keys of the stretchable keyboard, that is up, down, left, right, blank (middle), and heater switch (bottom left). (C) Schematic diagram of the wireless e-skin human-machine interactive system. (D) Application of the NHSE-based e-skin human-machine interactive system in controlling computer games on hand. (E, F) The robustness of the NHSE-based human-machine interactive system upon stretching and bending. (G) The temperature profiles of the NHSE-based serpentine heater under the voltages of 1, 2, 2.5, 3, 3.5, and 4 V. (H) Temperature evolution of the serpentine heater as applied 0%, 20%, 40%, 60%, 80%, and 100% strain at a constant voltage (1 V). The insets illustrate the corresponding IR images of different strains. (I) The temperature of the heater under repeated heating cycles at a constant voltage (3 V). (J) Photographs of a selectively activated line on the LNCS connected with LED under original, cutting, hole punching status. (K) Photograph of the damaged circuit upon stretching

exercising, and taking a shower. In addition, the NHSE promises two accesses in partial activation and laser cutting processing, through which an integrated healthcare

and human machine interactive system is demonstrated. More importantly, the robustness of the circuits is further evidenced by the instant reconstruction of the conductive

pathway after severe mechanical damages. This process is completed spontaneously without any manual repair or external heat. All of these demonstrate its promising potential in the application of long-term reliable e-skin or in vivo biocompatible components with ingenious structure designs, for example, air-permeable epidermal signal collectors, brain-machine interfaces, neural interfaces, and wound healing accelerators, which will be the focus of future investigations.

4 | EXPERIMENTAL SECTION

4.1 | Materials for the composite

(1) EGaIn eutectic alloy was fabricated by mixing high-purity metal gallium (99.99%; Beijing Founde Star Sci. & Technol. Co., Ltd.) and indium (99.995%; Beijing Founde Star Sci. & Technol. Co., Ltd.) in a ratio of 75.5 and 24.5 wt.%, respectively. (2) The TPU solution was prepared by dissolving TPU (Sigma-Aldrich) in hexafluoroisopropanol (HFIP, Aladdin) at a weight percentage of 4% and then stirred for 8 h at room temperature.

4.2 | Preparation of the NHSE

The EGaIn suspension was prepared by sonicating 2.25 g of bulk EGaIn eutectic alloy in 12.75 g of isopropanol alcohol for 10 min in a 20 ml vial, conducted in ultrasonic cell disruption system at 50% amplitude (Ymnl-1000Y, Nanjing Immanuel Instrument Equipment Co.). The vial was placed in an ice bath in this process to reduce solvent evaporation. Subsequently, the liquid metal slurry, separated from the lighting suspension after standing for 20 min, was transferred into a 5 ml syringe with a 19 G metallic nozzle (Bodunbaili Co., Ltd.). In addition, the homogeneous TPU solution was transferred into a plastic syringe equipped with a 26 G metallic nozzle. The EGaIn and TPU solution syringes were fitted on a syringe pump for electrospaying and electrospinning on an electrospinning device (Beijing Tech Nova TEADFS-103), respectively. The TPU nanofiber was produced with a positive voltage of 9 kV, and the EGaIn slurry was sprayed uniformly on the TPU nanofiber with a positive voltage of 11 kV, which were both collected on a revolving roller wrapped with aluminum foil with a negative voltage of 2 kV. The needle-collector distances were 15 cm and 10 cm for TPU and EGaIn, respectively. Then pump rate for TPU electrospinning and EGaIn electrospaying was adjusted to be 0.04 and 0.02–0.08 ml min⁻¹, respectively. The as-fabricated LM nanoparticle/TPU scaffold composite

(LNSC) film was transferred to a 100 μm Polyethylene terephthalate (PET) film for further device fabrication and property characterization.

4.3 | Measurement of LM mass loading and volume ratio

The blank control (TPU scaffold without LM) and samples with various electrospaying rates of LM were cut to a size of 1 cm × 1 cm and weighed. Because the mass of the experimental samples is composed of the mass of the LM and TPU scaffold substrate, the weight of the LM (m_{LM}) and mass loading of the LM (ϵ) were calculated as follows:

$$m_{LM} = m_e - m_b, \quad (1)$$

$$\epsilon = \frac{m_{LM}}{m_e}, \quad (2)$$

where m_e and m_b are the weights of the experimental samples and blank control, respectively. Here, we assume that the mass loading variation of the LM nanoparticles has a negligible impact on the volume of the samples. The density (d_{LM}) of the LM was measured as 6.25 g cm⁻³. Therefore, the volume ratio of the LM (λ) can be calculated by

$$\lambda = \frac{V_{LM}}{V_e} = \frac{m_{LM}}{d_{LM} V_e}, \quad (3)$$

where V_{LM} and V_e are the volumes of the LM and the experimental samples, respectively. Therefore, ϵ and λ in samples with various parameters can be calculated using Equations (1)–(3).

4.4 | Activation of electrical circuit and electrode

The LNSC was activated by drawing a line with a rubber tip to form a circuit and scraping with a PET patch to fabricate a plane electrode. The pressure applied to the sample induces the rupturing of oxide shells on the LM nanoparticles and the formation of the circuit or electrode mechanically. For the capacitive sensor array, a PET mask was applied on the surface of the LNSC, and a brush was used to scrape the exposed area. The NHSE-based serpentine heater was fabricated by cutting the NHSE with designed patterns using a commercial laser cutter.

4.5 | Stretchable heater measurement

The NHSE-based serpentine heater was equipped on a stepping motor with a voltage supplied by a DC power. The temperature variation of the sample was captured using an infrared thermal image camera (T630sc, FLIR).

4.6 | Microstructure characterization

The surface and cross-sectional microstructures of the NHSE were characterized by field-emission SEM (SEM Sirion, FEI). The distribution of the elements (Ga and In) was identified by energy-dispersive X-ray spectroscopy (EDS, GENESIS).

4.7 | Electrical characterization

(1) Sheet resistance: The sheet resistance of the NHSE with different electro-spraying speeds was measured by a four-probe resistivity measurement system (Guangzhou 4-probe Tech Co. Ltd., RTS-9). (2) Electric resistance: 1 cm × 1 cm samples were prepared for electrical resistance measurements in single stretching and cyclic stretching. Moreover, 2 cm × 1 cm patches were fabricated for electrical resistance measurements during bending. Further, 3 cm × 1 cm patches on a 100 μm thick polydimethylsiloxane film were fabricated for electrical resistance measurement during twisting. A conductive copper wire was pasted on the ends of each sample using a silver paste. The electrical resistance of the NHSE was monitored by a digital sourcemeter (Keithley 2611 B) using a standard four-point method. (3) Contact impedance measurement: Two NHSE patches (16 mm in diameter) were prepared and attached to the forearms wetted with ethanol. The center-to-center distance of the two NHSE patches was maintained at 5 cm. The electrode-skin contact impedance was measured using an electrochemical analyzer (CHI660E) over a frequency range of 1–10⁵ Hz. For the control group, a gel electrode (Ag/AgCl) from the medical health care system (Heal Force PC-3000) was applied, and all the experimental parameters were unchanged.

4.8 | In vitro biocompatibility test

The live/dead assay was performed using the LIVE/DEAD Viability/Cytotoxicity Kit for mammalian cells (Invitrogen) according to the manufacturer's protocol. The NHSE film was soaked in a cell for 24 h at a concentration of 2.5 mg ml⁻¹. The human dermal fibroblast cell

line was cultured in 96 well plates, and the culture medium was replaced with the previously extracted medium for 24 h before staining. The combined viability assay reagent consisting of calcein AM (2 μM) and ethidium homodimer-1 (4 μM) was used to dye the cells. The labeled cells were captured under a confocal microscope (Leica DMI8).

4.9 | ECG measurement

Two NHSE patches (16 mm in diameter with a 3 cm tail) were prepared and attached to each forearm, and another (16 mm in diameter with a tail) NHSE patch was pasted at 2 cm above the ankle of the left leg. Then, the conductive textile (lead wire) was pasted onto the tail of the NHSE with the assistance of the silver paste and a tape (3M) that maintained a good connection between the lead wire and patches electrically and geometrically. Subsequently, the lead wires were connected to a commercial health monitoring machine (Heal Force PC-3000) for ECG measurements. For the control group, gel electrodes (Ag/AgCl) were applied for ECG monitoring, and all the experimental parameters above were unchanged.

ACKNOWLEDGMENTS

This research was supported by Ningbo Municipal 3315 Talent Scheme by Ningbo Science and Technology Bureau, the Zhejiang Provincial Natural Science Foundation of China (Grant No. LR19F010001), the National Key R & D Project from Ministry of Science and Technology, China (Grant Nos. 2016YFA0202703), National Natural Science Foundation of China (Grant Nos. 51525103, 51701231 and 51931011), K.C. Wong Education Foundation (Grant No. GJTD-2020-11).

CONFLICT OF INTEREST

The authors declare no conflict of interest.

DATA AVAILABILITY STATEMENT

All data needed to evaluate the conclusions in the paper are present in the paper and/or the Supporting Information. Additional data related to this paper may be requested from the corresponding authors.

ORCID

Guang Zhu  <https://orcid.org/0000-0003-2350-0369>

Run-Wei Li  <https://orcid.org/0000-0003-3879-9834>

REFERENCES

1. Matsuhisa N, Inoue D, Zalar P, et al. Printable elastic conductors by in situ formation of silver nanoparticles from silver flakes. *Nat Mater*. 2017;16(8):834-840.

- Choi S, Han SI, Jung D, et al. Highly conductive, stretchable and biocompatible Ag–Au core-sheath nanowire composite for wearable and implantable bioelectronics. *Nat Nanotechnol.* 2018;13(11):1048-1056.
- Cheng T, Zhang YZ, Wang S, et al. Conductive hydrogel-based electrodes and electrolytes for stretchable and self-healable supercapacitors. *Adv Funct Mater.* 2021;31(24):2101303.
- Li S, Zhang Y, Wang Y, et al. Physical sensors for skin-inspired electronics. *InfoMat.* 2019;2(1):184-211.
- Liu J, Zhang X, Liu Y, et al. Intrinsically stretchable electrode array enabled in vivo electrophysiological mapping of atrial fibrillation at cellular resolution. *Proc Natl Acad Sci U S A.* 2020;117(26):14769-14778.
- Kang SK, Murphy RK, Hwang SW, et al. Bioresorbable silicon electronic sensors for the brain. *Nature.* 2016;530(7588):71-76.
- Li D, Lai W-Y, Zhang Y-Z, Huang W. Printable transparent conductive films for flexible electronics. *Adv Mater.* 2018;30(10):1704738.
- Zhou L, Yu M, Chen X, et al. Screen-printed poly(3,4-ethylenedioxythiophene):poly(styrenesulfonate) grids as ITO-free anodes for flexible organic light-emitting diodes. *Adv Funct Mater.* 2018;28(11):1705955.
- Minev IR, Musienko P, Hirsch A, et al. Electronic dura mater for long-term multimodal neural interfaces. *Science.* 2015;347(6218):159-163.
- Cheng T, Wu YW, Chen YL, Zhang YZ, Lai WY, Huang W. Inkjet-printed high-performance flexible micro-supercapacitors with porous nanofiber-like electrode structures. *Small.* 2019;15(34):1901830.
- Markvicka EJ, Bartlett MD, Huang X, Majidi C. An autonomously electrically self-healing liquid metal-elastomer composite for robust soft-matter robotics and electronics. *Nat Mater.* 2018;17(7):618-624.
- Jiang Z, Nayeem MOG, Fukuda K, et al. Highly stretchable metallic nanowire networks reinforced by the underlying randomly distributed elastic polymer nanofibers via interfacial adhesion improvement. *Adv Mater.* 2019;31(37):1903446.
- Miyamoto A, Lee S, Cooray NF, et al. Inflammation-free, gas-permeable, lightweight, stretchable on-skin electronics with nanomeshes. *Nat Nanotechnol.* 2017;12(9):907-913.
- Norton JJS, Lee DS, Lee JW, et al. Soft, curved electrode systems capable of integration on the auricle as a persistent brain-computer interface. *Proc Natl Acad Sci U S A.* 2015;112(13):3920-3925.
- Matsuhisa N, Chen X, Bao Z, Someya T. Materials and structural designs of stretchable conductors. *Chem Soc Rev.* 2019;48(11):2946-2966.
- Dickey MD. Stretchable and soft electronics using liquid metals. *Adv Mater.* 2017;29(27):1606425.
- Cheng T, Zhang Y, Lai WY, Huang W. Stretchable thin-film electrodes for flexible electronics with high deformability and stretchability. *Adv Mater.* 2015;27(22):3349-3376.
- Wang C, Zhang M, Xia K, et al. Intrinsically stretchable and conductive textile by a scalable process for elastic wearable electronics. *ACS Appl Mater Interfaces.* 2017;9(15):13331-13338.
- Zhang Y, Sheehan CJ, Zhai J, et al. Polymer-embedded carbon nanotube ribbons for stretchable conductors. *Adv Mater.* 2010;22(28):3027-3031.
- Jang KI, Li K, Chung HU, et al. Self-assembled three dimensional network designs for soft electronics. *Nat Commun.* 2017;8(1):15894.
- Wang Y, Zhu C, Pfattner R, et al. A highly stretchable, transparent, and conductive polymer. *Sci Adv.* 2017;3(3):1602076.
- Jin H, Matsuhisa N, Lee S, Abbas M, Yokota T, Someya T. Enhancing the performance of stretchable conductors for E-textiles by controlled ink permeation. *Adv Mater.* 2017;29(21):1605848.
- Daeneke T, Khoshmanesh K, Mahmood N, et al. Liquid metals: fundamentals and applications in chemistry. *Chem Soc Rev.* 2018;47(11):4073-4111.
- Yu Z, Shang J, Niu X, et al. A composite elastic conductor with high dynamic stability based on 3D-Calabash bunch conductive network structure for wearable devices. *Adv Electron Mater.* 2018;4(9):1800137.
- Ma B, Xu C, Chi J, Chen J, Zhao C, Liu H. A versatile approach for direct patterning of liquid metal using magnetic field. *Adv Funct Mater.* 2019;29(28):1901370.
- Tavakoli M, Malakooti MH, Paisana H, et al. EGaIn-assisted room-temperature sintering of silver nanoparticles for stretchable, inkjet-printed, thin-film electronics. *Adv Mater.* 2018;30(29):1801852.
- Hirsch A, Michaud HO, Gerratt AP, de Mulatier S, Lacour SP. Intrinsically stretchable biphasic (solid-liquid) thin metal films. *Adv Mater.* 2016;28(22):4507-4512.
- Guo R, Sun X, Yuan B, Wang H, Liu J. Magnetic liquid metal (Fe-EGaIn) based multifunctional electronics for remote self-healing materials, degradable electronics, and thermal transfer printing. *Adv Sci.* 2019;6(20):1901478.
- Park JE, Kang HS, Koo M, Park C. Autonomous surface reconciliation of a liquid-metal conductor micropatterned on a deformable hydrogel. *Adv Mater.* 2020;32(37):2002178.
- Sekitani T, Nakajima H, Maeda H, et al. Stretchable active-matrix organic light-emitting diode display using printable elastic conductors. *Nat Mater.* 2009;8(6):494-499.
- Shi G, Zhao Z, Pai J-H, et al. Highly sensitive, wearable, durable strain sensors and stretchable conductors using graphene/silicon rubber composites. *Adv Funct Mater.* 2016;26(42):7614-7625.
- Fan YJ, Yu PT, Liang F, et al. Highly conductive, stretchable, and breathable epidermal electrode based on hierarchically interactive nano-network. *Nanoscale.* 2020;12(30):16053-16062.
- Mohammed MG, Kramer R. All-printed flexible and stretchable electronics. *Adv Mater.* 2017;29(19):1604965.
- Ma Z, Huang Q, Xu Q, et al. Permeable superelastic liquid-metal fibre mat enables biocompatible and monolithic stretchable electronics. *Nat Mater.* 2021;20(6):859-868.
- Liu L, Li HY, Fan YJ, et al. Nanofiber-reinforced silver nanowires network as a robust, ultrathin, and conformable epidermal electrode for ambulatory monitoring of physiological signals. *Small.* 2019;15(22):1900755.
- Park S, Thangavel G, Parida K, Li S, Lee PS. A stretchable and self-healing energy storage device based on mechanically and electrically restorative liquid-metal particles and carboxylated polyurethane composites. *Adv Mater.* 2019;31(1):1805536.
- Li X, Li M, Xu J, You J, Yang Z, Li C. Evaporation-induced sintering of liquid metal droplets with biological nanofibrils for

- flexible conductivity and responsive actuation. *Nat Commun.* 2019;10(1):3514.
38. Lopes PA, Paisana H, De Almeida AT, Majidi C, Tavakoli M. Hydroprinted electronics: ultrathin stretchable Ag–In–Ga E-skin for bioelectronics and human–machine interaction. *ACS Appl Mater Interfaces.* 2018;10(45):38760–38768.
39. Tybrandt K, Khodagholy D, Dielacher B, et al. High-density stretchable electrode grids for chronic neural recording. *Adv Mater.* 2018;30(15):1706520.
40. Park S-M, Jang N-S, Ha S-H, et al. Metal nanowire percolation micro-grids embedded in elastomers for stretchable and transparent conductors. *J Mater Chem C.* 2015;3(31):8241–8247.
41. Hong S, Lee H, Lee J, et al. Highly stretchable and transparent metal nanowire heater for wearable electronics applications. *Adv Mater.* 2015;27(32):4744–4751.
42. Li J, Qi S, Liang J, et al. Synthesizing a healable stretchable transparent conductor. *ACS Appl Mater Interfaces.* 2015;7(25):14140–14149.
43. Du X, Jiang W, Zhang Y, et al. Transparent and stretchable graphene electrode by intercalation doping for epidermal electrophysiology. *ACS Appl Mater Interfaces.* 2020;12(50):56361–56371.
44. Kim BS, Kwon H, Kwon HJ, et al. Buckling instability control of 1D nanowire networks for a large-area stretchable and transparent electrode. *Adv Funct Mater.* 2020;30(21):1910214.
45. Hyun DC, Park M, Park C, et al. Ordered zigzag stripes of polymer gel/metal nanoparticle composites for highly stretchable conductive electrodes. *Adv Mater.* 2011;23(26):2946–2950.
46. Wei Y, Chen S, Yuan X, Wang P, Liu L. Multiscale wrinkled microstructures for piezoresistive fibers. *Adv Funct Mater.* 2016;26(28):5078–5085.
47. Li W, Matsuhisa N, Liu Z, et al. An on-demand plant-based actuator created using conformable electrodes. *Nat Electron.* 2021;4(2):134–142.
48. Zheng R, Wu Y, Xu Y, et al. Advanced stretchable characteristic of liquid metal for fabricating extremely stable electronics. *Mater Lett.* 2019;235:133–136.
49. Ryu J, Kim J, Oh J, et al. Intrinsically stretchable multifunctional fiber with energy harvesting and strain sensing capability. *Nano Energy.* 2019;55:348–353.
50. Zhuang Q, Ma Z, Gao Y, et al. Liquid–metal–superlyophilic and conductivity–strain-enhancing scaffold for permeable superelastic conductors. *Adv Funct Mater.* 2021;47:2105587.
51. Khan MR, Trlica C, Dickey MD. Recapillarity: electrochemically controlled capillary withdrawal of a liquid metal alloy from microchannels. *Adv Funct Mater.* 2015;25(5):671–678.
52. Ayres CE, Jha BS, Meredith H, et al. Measuring fiber alignment in electrospun scaffolds: a user's guide to the 2D fast Fourier transform approach. *J Biomater Sci Polym Ed.* 2008;19(5):603–621.
53. Boley JW, White EL, Kramer RK. Mechanically sintered gallium–indium nanoparticles. *Adv Mater.* 2015;27(14):2355–2360.
54. Kabiri Ameri S, Ho R, Jang H, et al. Graphene electronic tattoo sensors. *ACS Nano.* 2017;11(8):7634–7641.
55. Yang H, Ji S, Chaturvedi I, et al. Adhesive biocomposite electrodes on sweaty skin for long-term continuous electrophysiological monitoring. *ACS Mater Lett.* 2020;2(5):478–484.

SUPPORTING INFORMATION

Additional supporting information may be found in the online version of the article at the publisher's website.

How to cite this article: Cao J, Liang F, Li H, et al. Ultra-robust stretchable electrode for e-skin: In situ assembly using a nanofiber scaffold and liquid metal to mimic water-to-net interaction. *InfoMat.* 2022;4(4):e12302. doi:10.1002/inf2.12302